Supplemental Material for:

Depth-resolved Optical Imaging and Microscopy of Vascular Compartment Dynamics During Somatosensory Stimulation

Elizabeth M. C. Hillman[1], Anna Devor[1,2], Matthew Bouchard[1], Andrew K. Dunn[3], GW Krauss[1], Jesse Skoch[4], Brian J. Bacskai[4], Anders M. Dale[2] and David A. Boas[1]

[1]Athinoula A. Martinos Center for Biomedical Imaging, [4]Neurology, Massachusetts General Hospital, Building 149, 13th Street, Charlestown, Massachusetts 02129.

[2]Neuroscience and Radiology, University of California San Diego, 9500 Gillman Drive, La Jolla, California 92093.

[3]Biomedical Engineering, University of Texas at Austin, 1 University Station, C0800, Austin, TX 78712

Contents:

- **Fig.S1.** Depth-resolved hemodynamic imaging. (Same as Fig 2. for a second rat).
- **Fig S2.** 3D Spatiotemporal Separation of Vascular Compartments. (Same as Fig 3. for a second rat).
- **Fig S3.** Objective masking rather than subjective selection of arteriole, capillary and vein regions.
- **Fig S4.** Residuals of spatiotemporal fit and singular value decomposition analysis.
- **Fig S5.** Higher resolution plots of the average hemodynamic trends extracted from the 5 rats (compartments).
- **Fig S6.** Higher resolution plots of the average hemodynamic trends extracted from the 5 rats (hemoglobin types).
- **Supplemental Methods I:** Data processing and image reconstruction for Laminar Optical Tomography.
- **Supplemental Methods II:** Extraction of parameters from in-vivo two-photon data.

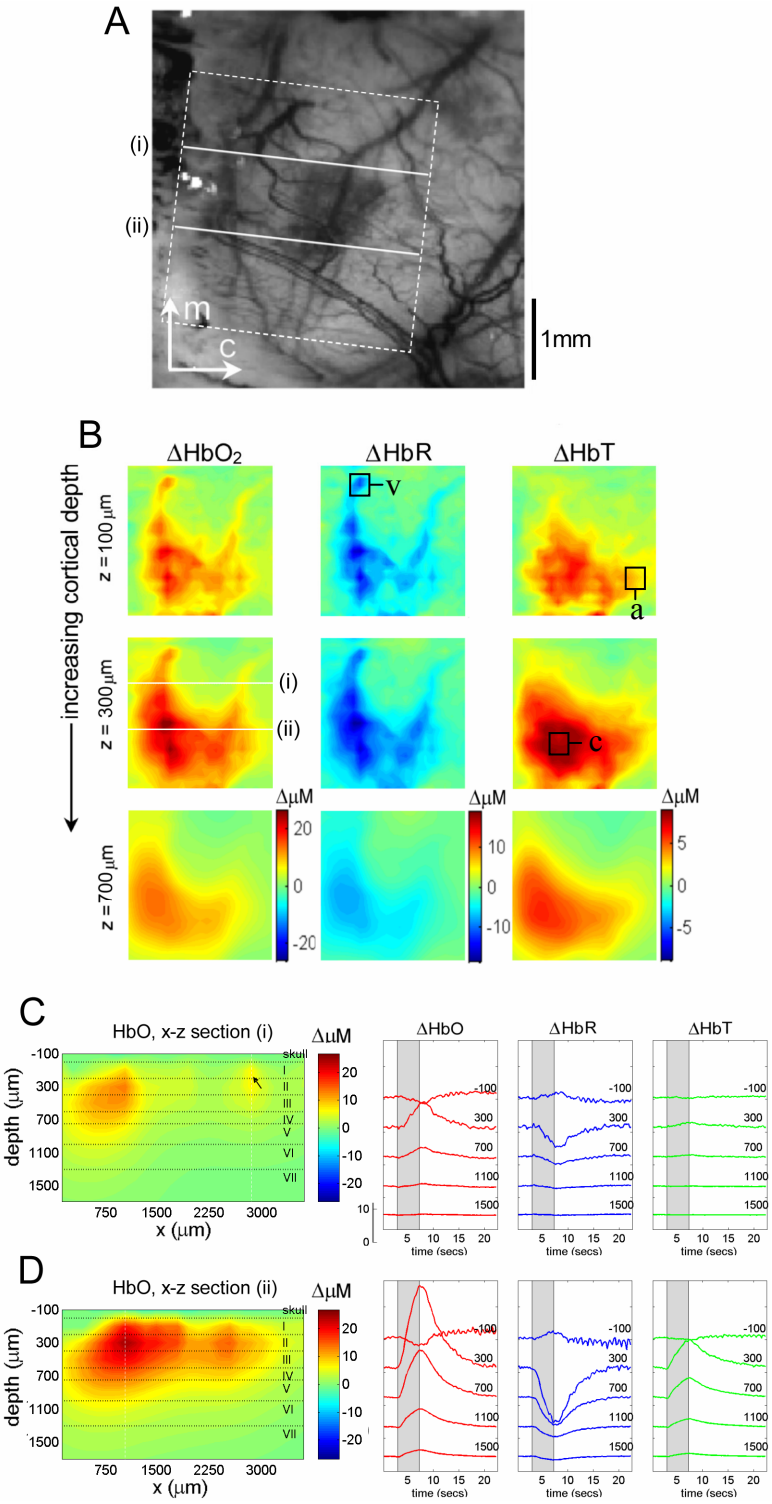

Fig.S1. Depth-resolved hemodynamic imaging. Same as FIG 2. for a second rat.
A) shows the CCD image of rat cortical surface through thinned skull. The region imaged using LOT is indicated by the white dotted lines. B) Shows depth-resolved LOT images of oxy-, deoxy-and total hemoglobin concentration changes in the cortex 0.6 seconds after cessation of a 4 second forepaw stimulus at cortical depths of 100, 300 and 700 microns. C) shows a depth-resolved cross section of the HbO_2 response at the position indicated with (i) in B representing a large draining vein. The corresponding HbO_2, HbR and HbT depth-resolved time-courses around x = 2850microns are shown to the right. D) shows a depth-resolved cross section of the HbO_2 response at the position indicated with (ii) in B. The corresponding HbO_2, HbR and HbT depth-resolved time-courses around x = 1050microns are shown to the right. Numbers on each temporal trace represent their depth of origin in microns. 'a','v' and 'c' denote regions identified as arteriole, vein and capillary for timecourse extraction.

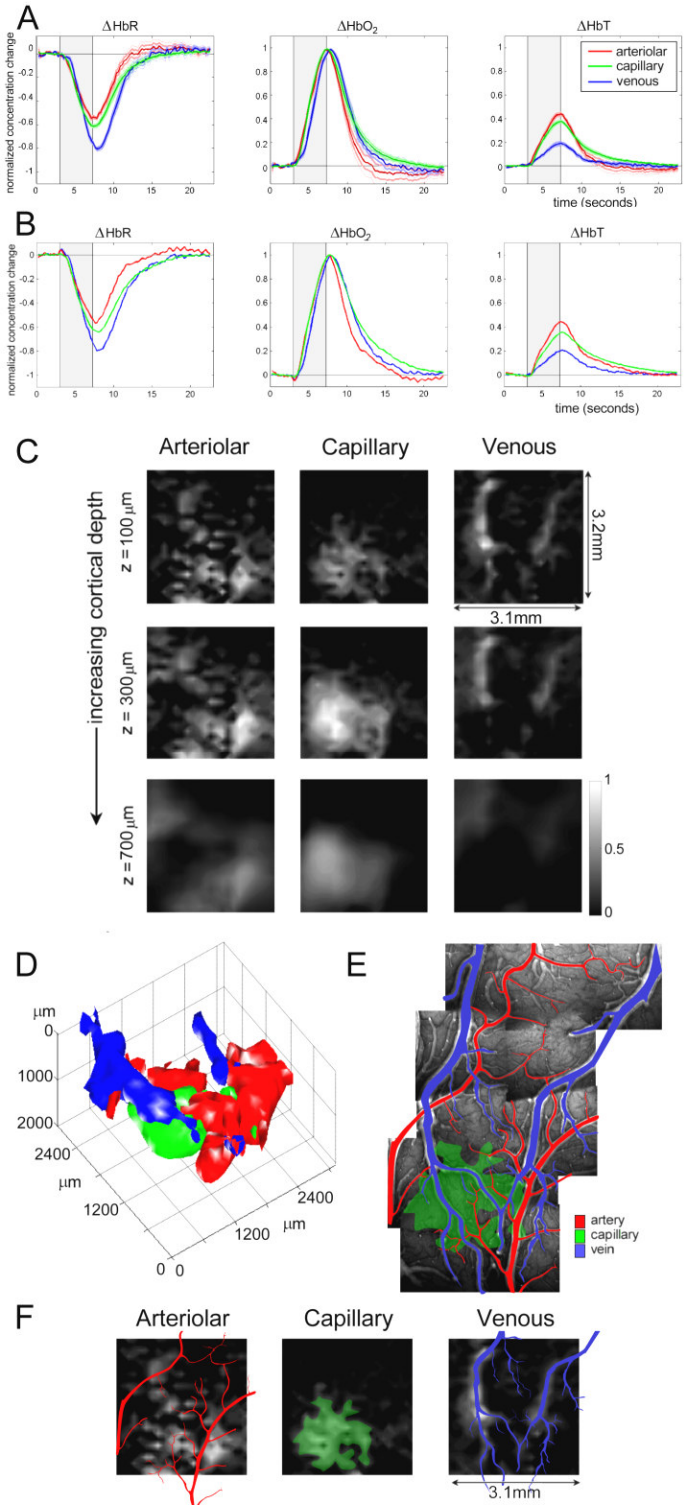

Fig S2. 3D Spatiotemporal Separation of Vascular Compartments. (Same as FIG 3. for a second rat).
A) The average hemodynamic time-courses over 5 rats isolated from voxels in the LOT images expected to represent arteriolar, capillary and venous contributions. (normalized to the peak HbO_2 value). B) Equivalent time courses for the rat shown in Fig. S1. C) Spatiotemporal components extracted from the 3D LOT data shown in figure S1B. Gray scale represents the amplitude of the component in each voxel that varies according to the arterial, capillary and venous functional time-courses shown in B. D) 3D rendering of LOT vascular compartments (40% isosurface). E) 2-photon image stack of fluorescent vascular cast with veins (blue) and arteries / arterioles (red) identified. F) 200 micron depth slice from C overlaid with the tracing of the arteries (red) and veins (blue) from the vascular cast (after rotation and scaling). The capillary response from the LOT results is overlaid onto the vascular cast image to indicate the position of the active underlying capillary bed (green).

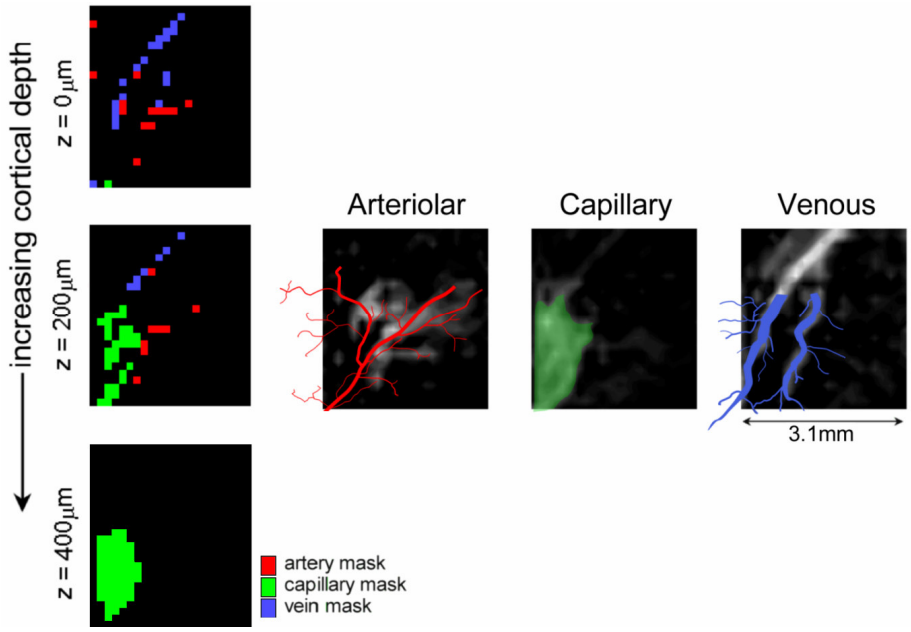

Fig S3a). Objective masking rather than subjective selection of arteriole, capillary and vein regions. (Left) the result of objective masking of LOT data based on only the general characteristics of the vascular compartment timecourses. Voxels were searched to identify regions that had only the basic temporal characteristics of each vascular compartment. The regions identified correspond well to the regions initially selected subjectively and to those subsequently identified with two-photon microscopy (right). The timecourses extracted from the LOT data from the regions identified in each mask closely resembled those extracted via subjective selection.

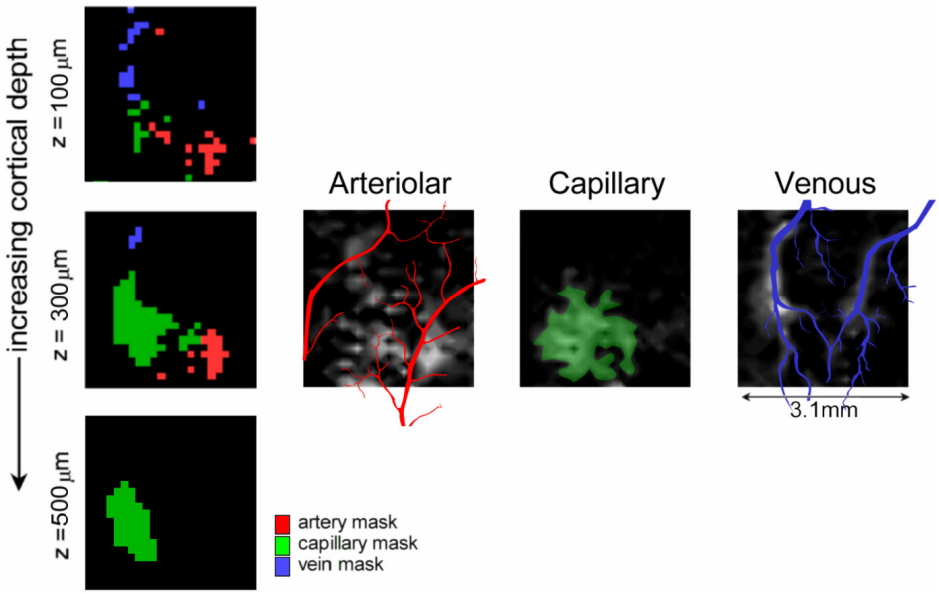

Fig S3b). Same as FIG S3a for a second rat.

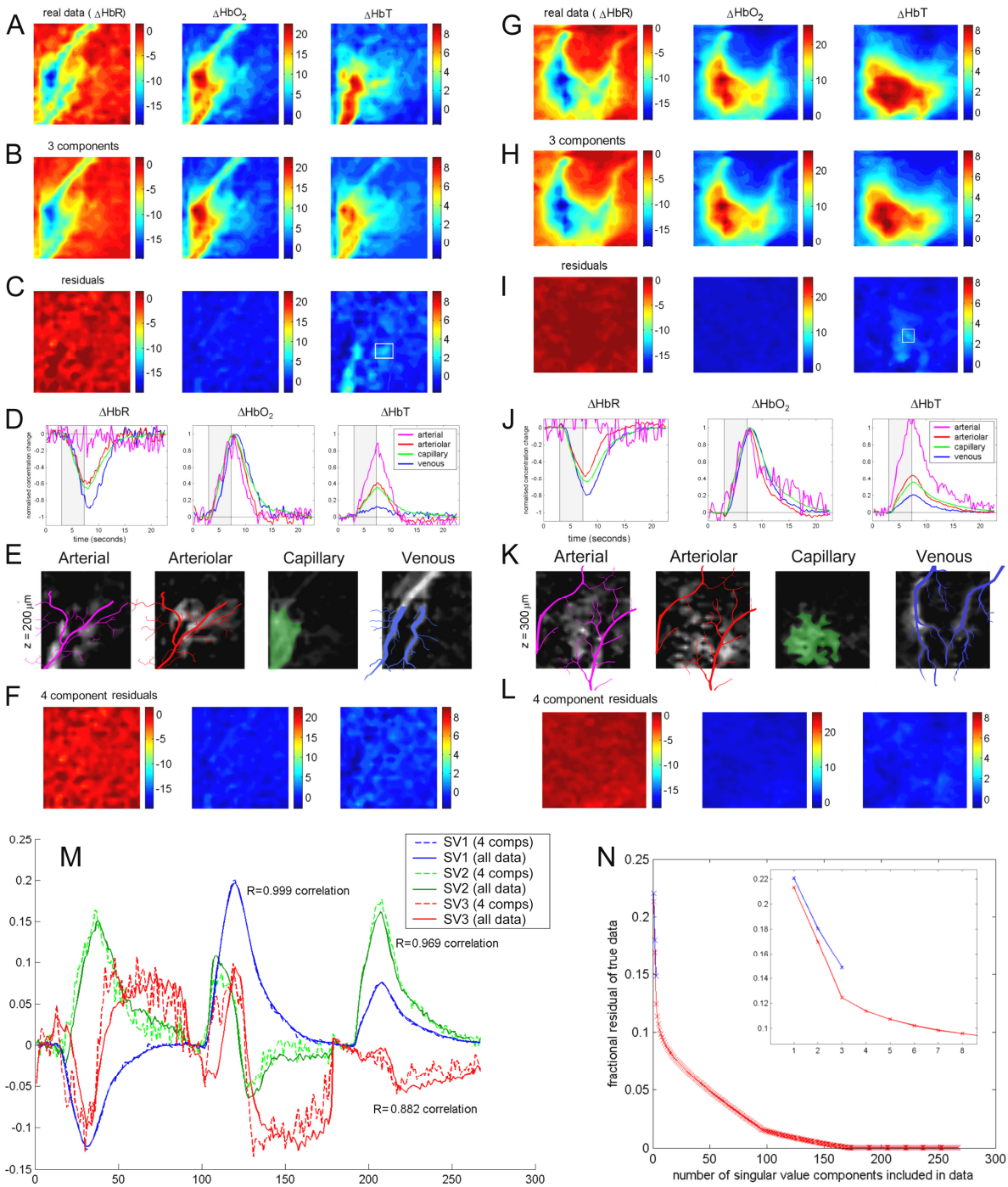

Fig S4 Residuals of spatiotemporal fit and singular value decomposition analysis: A) a slice from the original LOT HbR, HbO_2 and HbT images for the rat shown in Fig 1. B) The same plane when re-formed using only the 3 basis time-courses and the spatial component images from Fig2. C) = (A-B), the residual of the 3 component fit relative to the true data (on the same color-scale). D) The time-courses of the original 3 temporal components (arteriolar, capillary and venous) in addition to a magenta trace showing the time-course of the (white box) region in the HbT residual, thought to correspond to a larger artery. E) The overlaid vascular architecture from the vascular casts shown in Fig2, including the arterial component from a 4-component temporal fit using the traces from D. F) the residuals of the images when the 4th arterial temporal component is incorporated into the spatiotemporal fit. G-L are the same data for a second rat (that shown in figure S1). M) Shows the first three singular values of the complete 3D image data set, overlaid with the first three singular values of the four basis temporal components shown in J. N) Shows the residual spectrum of the data set, showing the fractional residual between the full data set and data created from a gradually increasing number of singular values (red). The small blue trace shows the residual when the first three singular values of the 4-component subset are used in place of the whole data set singular values (insert shows close up). This analysis shows that the 4 vascular compartment timecourses can account for around 85% of all variance in the 3D data.

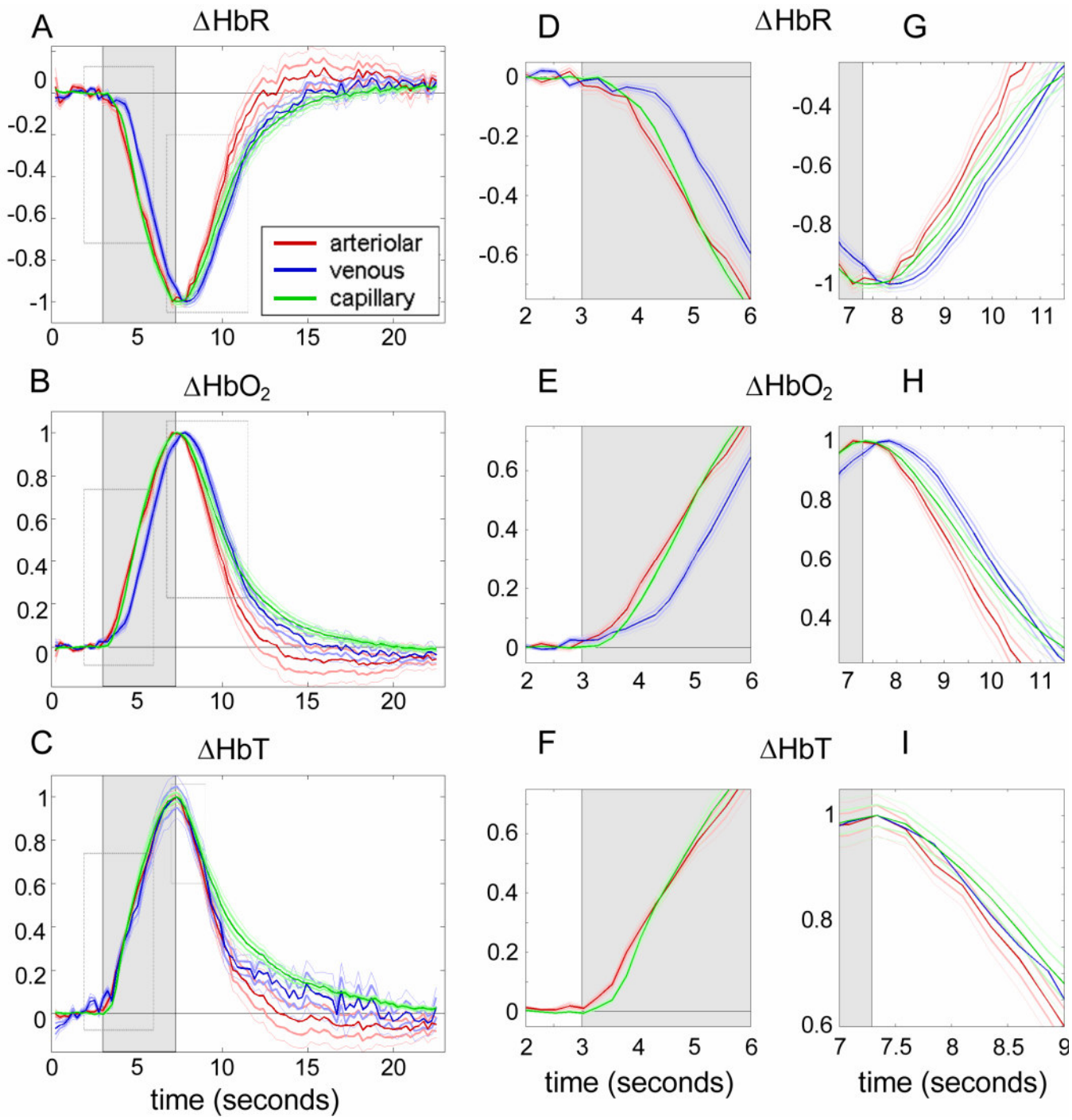

Fig S5. Higher resolution plots of the average hemodynamic trends extracted from the 5 rats (error bounds represent the standard deviation on the mean of the data after normalization to the peak of the HbO_2 response). Here, data has been normalized to the peak of each hemoglobin form. The central and right columns show close ups of the onset and decay of each trace respectively.

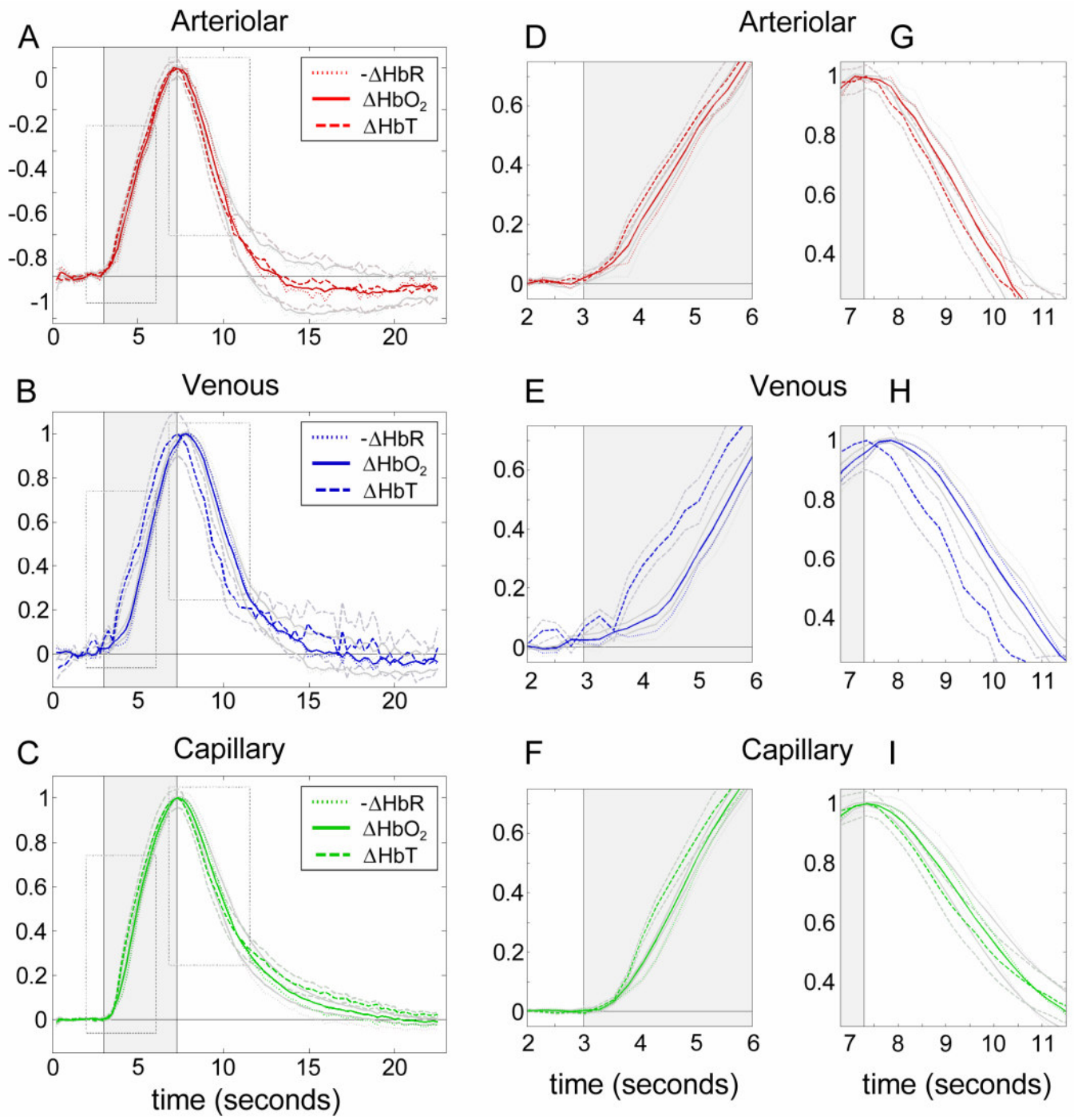

Fig S6 Higher resolution plots of the average hemodynamic trends extracted from the 5 rats (error bounds represent the standard deviation on the mean of the data after normalization to the peak of the HbO_2 response). Here, data has been normalized to the absolute peak of each vascular compartment. The central and right columns show close ups of the onset and decay of each trace respectively.

Supplemental methods I: Data processing and image reconstruction for LOT.

LOT data pre-processing

All data acquisition and processing was performed using Matlab™ software. For each stimulus block, 90 LOT image frames were acquired at each wavelength (473nm or 532nm) during the first 23 seconds (including 3 seconds pre-stimulus, 4 seconds stimulus and 16 seconds post-stimulus, with a 27 second inter-stimulus interval). Between 140 and 500 separate stimulus blocks were recorded for each rat. The responses in the raw data were examined alongside simultaneously acquired physiology data, and the corresponding absolute images so that exclusion criteria could be applied. The remaining scans for each rat were then spatially co-registered using custom-written Matlab™ code which spatially shifted each frame to minimize its absolute difference relative to a reference frame. The data were then block-averaged and the percentage changes relative to pre-stimulus baseline were calculated for all images of each wavelength: Where $M_{s,Dark}$ is a measurement of the signal on each detector when the focused laser beam is deflected into a beam-dump, the average stimulus response over N trials, for each detector *s*, and position p, over time *t* for each rat was calculated using:

$$\frac{\Delta M_{s,p}(t)}{M_{s,p}(0)} = \frac{1}{N}\sum_{n=1}^{N}\left(\frac{M_{s,p}(n,t) - \frac{1}{12}\sum_{t=1}^{12} M_{s,p}(n,t)}{\frac{1}{12}\sum_{t=1}^{12} M_{s,p}(n,t) - M_{s,p,Dark}}\right), \qquad [1]$$

where the resulting data represents the percentage change in signal relative to a baseline given by the mean of the 1st 12 time-points of each scan. No spatial or temporal filtering was used. Since the two wavelengths were acquired sequentially (100ms apart), the 473nm image series was then temporally linearly interpolated to the same time base as the 532nm images. The resulting dual-wavelength raw data time-series for each rat were then converted into 3D images of wavelength-specific absorption changes, and then subsequently converted into maps of ΔHbR, ΔHbO_2 and ΔHbT changes as described below.

Image reconstruction

Raw LOT data is converted into 3D images of wavelength-dependent absorption using a computed-tomography-like deconvolution procedure, based on Monte-Carlo modeling of light propagation in scattering tissue. This step is discussed in more detail in (Dunn and Boas, 2000; Hillman et al., 2004). Briefly, a linearized model (under the Born approximation: eq 2) is solved using Tikhonov regularization (eq 3) to produce 3D image timecourses of the change in absorption $\Delta\mu_a(\lambda_1,r,t)$ at each wavelength λ_1 and λ_2.

$$\Delta\mathbf{M} = \mathbf{J}\Delta\boldsymbol{\mu}_a \qquad [2]$$

$$\Delta\boldsymbol{\mu}_a = \mathbf{J}^{\mathbf{T}}(\mathbf{J}\mathbf{J}^{\mathbf{T}} + \alpha I)^{-1}\frac{\Delta\mathbf{M}\,\mathbf{L_0}}{\mathbf{M}_0} \qquad [3]$$

where $\Delta\mathbf{M}/\mathbf{M_0} = \Delta M_{s,p}(t)/M_{s,p}(0)$ (eq 1) is the set of percentage change LOT raw measurements. **J** are depth-sensitivity profiles (as shown in Fig 1) generated using Monte Carlo modeling. $\mathbf{L}_0$ is a factor representing the simulated baseline signal and was also calculated using the Monte Carlo model. Since LOT measurements are not within the diffusion regime, the angle of propagation of each photon was carefully taken into account. The Monte Carlo model also incorporated a 50 micron thick 'skull' layer and the background optical properties for the model were determined by systematic comparison between in-vivo rat LOT data (for 7 source-detector separations) and phantom measurements made on well-characterized mixtures of intralipid™ (a milk-like scattering solution) and bovine hemoglobin (Sigma Aldrich), with a thin sheet of wax paper

representing the skull. The following baseline optical properties were deduced and used: At 473nm: scattering coefficient: $\mu'_s = 0.56mm^{-1}$, absorption coefficient: $\mu_a = 0.38mm^{-1}$. At 532nm: $\mu'_s = 0.5mm^{-1}$, $\mu_a = 0.337mm^{-1}$. The skull was assumed to have $\mu'_s = 1mm^{-1}$, and $\mu_a = 0.1mm^{-1}$. Anisotropy of 0.9 was assumed.

The regularization parameter α was determined by calculating the variance of the in-vivo data (from steady-state sequences), adding this noise onto simulated data corresponding to a simple simulated shape (extending from 200 – 800 microns in depth), and then reconstructing this simulated data alongside the in-vivo data. When the simulated data reconstruction was accurate and neither reconstruction seemed over regularized, or overwhelmed by measurement noise the corresponding regularization parameter was selected. After review of the values for each rat, a common parameter was chosen and applied to the data from all rats.

Note that similar image reconstruction approaches have been well established for diffuse optical tomography (DOT)(Arridge, 1999). However, in the case of LOT, since the distances between source and detector positions are so small, image reconstruction is substantially more stable and produces much higher resolution images than conventional DOT. The final results of our reconstruction are 3D image timecourses of the change in absorption $\Delta\mu_a(\lambda_1,r,t)$ at each wavelength λ_1 = 532nm, and λ_2 = 473nm

Functional conversion

By explicitly converting the raw data into 3D absorption maps utilizing a model of light propagation that incorporates wavelength dependent, empirically determined optical properties of the rat brain, it is not necessary to account for partial volume effects or to estimate differential pathlength factors (Kohl et al., 2000). The resulting 3D $\Delta\mu_a(\lambda_1,r,t)$ images can be converted into absolute images of the mM changes in HbR, HbO_2 and HbT using the Beer Lambert law:

$$\Delta[HbO_2(r,t)] = \frac{\varepsilon_{HbR}(\lambda_2)\Delta\mu_a(\lambda_1,r,t) - \varepsilon_{HbR}(\lambda_1)\Delta\mu_a(\lambda_2,r,t)}{\varepsilon_{Hb}(\lambda_2)\varepsilon_{HbO}(\lambda_1) - \varepsilon_{HbO}(\lambda_2)\varepsilon_{Hb}(\lambda_1)}$$

$$\Delta[HbR(r,t)] = \frac{\varepsilon_{HbO}(\lambda_2)\Delta\mu_a(\lambda_1,r,t) - \varepsilon_{HbO}(\lambda_1)\Delta\mu_a(\lambda_2,r,t)}{\varepsilon_{HbO}(\lambda_2)\varepsilon_{HbR}(\lambda_1) - \varepsilon_{HbR}(\lambda_2)\varepsilon_{HbO}(\lambda_1)}$$

$$\Delta[HbT(r,t)] = \Delta[HbR(r,t)] + \Delta[HbO_2(r,t)] \qquad [4]$$

where $\Delta[HbO_2(r,t)]$ is a 3D image time-series of the oxy-hemoglobin concentration changes and $\varepsilon_{HbR}(\lambda_1)$ is the molar extinction coefficient of deoxy-hemoglobin at wavelength λ_1. The latter were obtained from published values http://omlc.ogi.edu/spectra/hemoglobin/summary.html. This process assumes that changes in hemoglobin are predominantly responsible for absorption changes in the brain at visible wavelengths (as is generally assumed in all 2D optical imaging studies).

Parameter extraction from compartment timecourses

Time to 30, 50 and 70% (onset and decay).

The peak amplitude was calculated as the mean of the 3 values either side of the peak of the response to avoid the influence of spikes. The 30, 50 or 70% of maximum threshold was then calculated and a quadratic fit to the points 0.7 to 1.3 times this threshold value was calculated. The intercept of this fit with the true threshold value was then calculated from the coefficients of the fit. Using a polynomial fit avoided the influence of spurious points or noise on the rising or falling slope of the data. While the algorithm was automated, it was carefully supervised to ensure that all fits and results reflected the true temporal behavior of each response.

Fractional contribution: sum of all voxels in each component.

Figure 5I was calculated from 3 of the 5 rats in this study owing to the incomplete field of view in the remaining animals (parts of the vascular response were obscured by the un-thinned parts of the skull). Estimates of the relative contribution of each compartment to the overall signal were obtained from the vascular compartment fit data (such as shown in figure 3C). Each value in these fit images represents the fraction to which the voxel behaves like a given compartment. We assume therefore that within the whole 3D sample, the highest (whitest) voxel is 100% composed of a particular compartment. The lowest voxel is always zero since a non-negative fit was used. Each 3D vascular compartment map was therefore normalized such that its maximum value was 1, and this normalization factor was applied to the functional time-courses used to generate the maps. The sum of all the values in the 3D map then represented the extent to which all the responding regions behaved like each given compartment. The relative amplitudes of the HbO_2, HbR and HbT responses for each compartment were calculated from the scaled functional time-courses that were the basis of the compartment fits. Each of these compartment-specific hemoglobin amplitudes were then multiplied by the totals from the spatial maps. In this way it was possible to calculate the fractional contribution of each compartment to the total response for each hemoglobin type. Standard deviations shown are between the three rats analyzed.

References

Arridge, S.R., 1999. Optical tomography in medical imaging. Inverse Problems 15pp. 41-93.

Dunn, A.K. and Boas, D.A., 2000. Transport-based image reconstruction in turbid media with small source–detector separations. Opt. Lett. 25(24), pp. 1777-1779.

Hillman, E.M.C., Boas, D.A., Dale, A.M. and Dunn, A.K., 2004. Laminar Optical Tomography: demonstration of millimeter-scale depth-resolved imaging in turbid media. Opt. Lett. 29(14), pp. 1650-1652.

Kohl, M., Lindauer, U., Royl, G., Kuhl, M., Gold, L., Villringer, A. and Dirnagl, U., 2000. Physical model for the spectroscopic analysis of cortical intrinsic optical signals. Phys Med Biol 45pp. 3749-3764.

Supplemental Methods II: Extraction of parameters from two-photon data:

Vessel diameter calculation

The orientation of the image was rotated to match vessel (using Matlab function "imrot"). The width at 0.4 of the peak value of the vessel cross section was determined from a linear interpolation of 3 adjacent points. Scaling was obtained by calibrating the field of view size using a 15 micron fluorescent microsphere phantom, and verified via successive translation of digitized x-y micrometer stage (typically 1.13 microns / pixel). Timing synchronization was determined by simultaneously recording stimulus triggers and galvanometer motion feedback signals (along with respiration and systemic blood pressure).

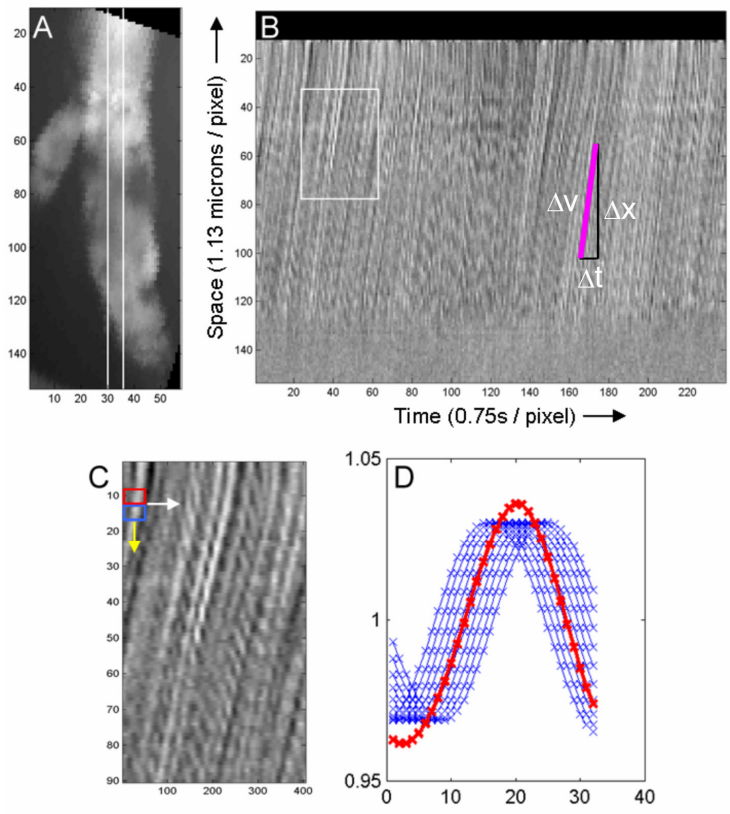

Speed of flow calculation

The orientation of image was rotated to match the vessel (using Matlab function "imrot") (A). The edges and length of the vessel were defined. 7 pixel wide stripes parallel to the vessel direction were averaged to create linescans (B) where the gradient of the stripes correspond to the speed of particle flow. The linescans were then spline interpolated to 10 x sample rate (7.5ms per new pixel) (C shows a close-up). A 30 x 4 (x by t) box (red) was then defined and its average timecourse compared to the timecourse of the 30 x 4 box below it. (blue). The t shift required to align the two represents the time taken for a red blood cell to travel 4 x-pixels (illustrated in D). These paired boxes are then moved temporally 10 points (0.75s to the right) and the process repeated, giving the measure of RBC speed at the next time-point. The paired boxes were then shifted down one x-pixel and the process repeated. The selected stripe of the vessel (A) was then shifted left-right across the vessel and the process repeated. All speed time-courses for all locations in the vessel were then averaged.

Red Blood Cell density calculation

The target vessel was selected, and histogram-based threshold used to determine an outline mask. All pixels outside mask were set to zero.

Each image in the time-series was then normalized such that the lowest value in vessel = 0 (100% red blood cells) and maximum value in vessel as 1 (no red blood cell – purely fluorescein in the plasma).
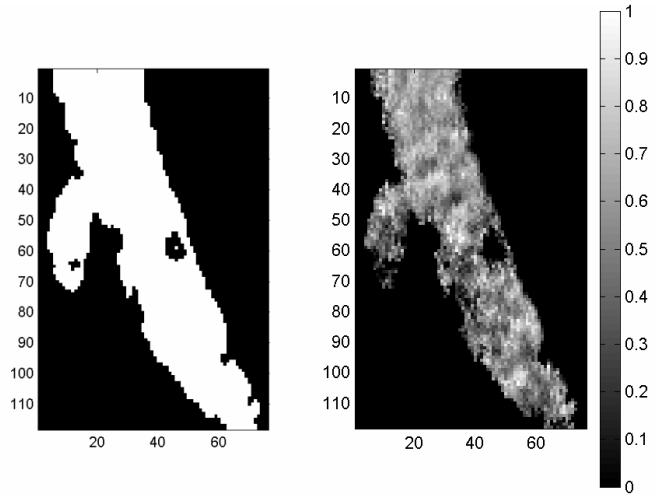
RBC density was then calculated as the sum of all pixel values in each masked, normalized image, divided by the number of pixels in the mask for each frame.